Journal of Solid State Chemistry **155,** 305–311 (2000)
doi:10.1006/jssc.2000.8918, available online at http://www.idealibrary.com on IDEAL®

Magnetic Properties of $BaMnS_2$ and $Ba_{0.93}Sr_{0.07}MnS_2$: Short-Range Magnetic Ordering Induced by Isovalent Substitution

Z. Serpil Gönen, James C. Fettinger, and Bryan Eichhorn

Department of Chemistry and Biochemistry, Center for Superconductivity Research, University of Maryland, College Park, Maryland 20742

Received August 1, 2000; in revised form July 25, 2000; accepted August 9, 2000; published online November 29, 2000

$BaMnS_2$ and $Ba_{0.93}Sr_{0.07}MnS_2$ were prepared from the binaries and elements at 1000°C. $Ba_{0.93}Sr_{0.07}MnS_2$ represents the limit of substitution in the $Ba_{1-x}Sr_xMnS_2$ solid solution and was characterized by single-crystal X-ray diffraction (orthorhombic, space group *Pnma*, $a = 7.109(2)$ Å, $b = 4.1069(13)$ Å, $c = 13.938(4)$ Å, $V = 407.0(2)$ Å^3, $Z = 4$), and wavelength dispersive X-ray spectroscopy. The compounds are isostructural, possessing a two-dimensional array of $MnS_{4/2}$ tetrahedra with channels of Ba/Sr atoms separating the layers. $BaMnS_2$ is antiferromagnetic with a suppressed moment at 300 K ($T_N > 380$ K). $Ba_{0.93}Sr_{0.07}MnS_2$ is also antiferromagnetic but shows short-range magnetic correlations between 230 and 70 K. *M* versus *H* curves at 100 K showed a small hysteresis. The $(Ba/Sr)^{2+}$ ions in $Ba_{0.93}Sr_{0.07}MnS_2$ are shifted to one side of the interlayer channels relative to $BaMnS_2$ and may be responsible for the anomalous magnetic behavior.

INTRODUCTION

Following the discovery of colossal magnetoresistance (CMR) in the manganese oxides, there has been renewed interest in valence precise and mixed valent manganese compounds (1–9). Although the CMR manganese oxides are usually high spin, mixed valent, and ferromagnetic (1), the CMR pnictides and sulfides have been shown to be antiferromagnetic (4, 5) and valence precise (10), respectively. Interest in the manganese CMR compounds stems not only from their potential applications but also from the variety of compositions and structures where the CMR effect is observed. It is not clear at present whether a single mechanism or different mechanisms are responsible for the CMR effect in the various compounds.

In an attempt to survey other mixed valent, potentially conductive/magnetic materials that are likely to show a magnetoresistance (MR) effect, we have studied the properties of the sulfide phases of V, Cr, Mn, and Fe. The mixed valent iron and manganese sulfides are particularly interesting due to their tendency to form high spin compounds that are reasonably conductive. The observation of a large CMR effect in $FeCr_2S_4$ is a case in point (10). MR effects in binary mixed valent chromium sulfides were documented 30 years ago (11). In addition, we recently described small MR effects in $BaFe_2S_3$ at low temperatures due to short-range magnetic correlations and spin glass like behavior (12). As an extension of this study, we have been investigating the properties of the manganese sulfides. The synthesis and structures of many of these compounds have been described by Bronger and others (13–18); however, many of the properties of these compounds remain unknown. We report here the properties of the Schmitz and Bronger compound $BaMnS_2$ (16, 17) and the isovalently substituted analog $Ba_{0.93}Sr_{0.07}MnS_2$. Although neither compound is a CMR material (they are both insulators), the latter shows an unusual short-range magnetic correlation that appears at 230 K but disappears at 70 K. The interactions appear to be induced by the isovalent substitution of Sr^{2+} for Ba^{2+}.

EXPERIMENTAL

Synthesis

All reagents were purchased from CERAC and used without further purification.

$BaMnS_2$. The compound was prepared according to two different procedures. In the first method from Schmitz and Bronger (16, 17) 0.391 g $BaCO_3$ (1.98 mmol) and 0.109 g Mn (1.98 mmol) were ground in air, placed in an alumina boat, and heated at 1000°C under flowing H_2S for 3 h. The sample was then cooled to room temperature under H_2S. In our hands, this procedure resulted in the formation of the title compound along with variable amounts of Ba_2MnS_3 (19) and MnS.

In an alternate synthesis, BaS (0.330 g, 1.95 mmol), Mn (0.107 g, 1.95 mmol), and S (0.063 g, 1.96 mmol) were ground and loaded into a silica ampule in a drybox and sealed under vacuum. The mixture was heated at 600°C for 83h using 1°C/min heating and cooling rates. The product was then reground and loaded into another silica ampule, and heated at 800°C for 17 h. The product was again

0022-4596/00 $35.00

reground and loaded into another silica ampule for the final heating at 1000°C for 50 h. The product was a microcrystalline orange powder that appeared to be single phase by X-ray diffraction (XRD) analysis.

$Ba_{0.93}Sr_{0.07}MnS_2$. BaS (0.303 g, 1.79 mmol), SrS (0.0238 g, 0.199 mmol), Mn (0.109 g, 1.98 mmol), and S (0.063 g, 1.99 mmol) were used to prepare the title compound according to the alternate synthetic method described above.

Characterization

Powder XRD patterns were obtained for both compounds using a Rigaku DMAX B powder X-ray diffractometer and an MDI software system. The purity of $BaMnS_2$ was assessed by way of Rietveld refinements of the XRD data according to standard methods used in our laboratory (20). The unit cell parameters and fractional coordinates from the single-crystal structure were used as the initial model. The unit cell parameters for $Ba_{0.93}Sr_{0.07}MnS_2$ were determined by least-squares analysis of the XRD data.

Single–crystal structure for $Ba_{0.93}Sr_{0.07}MnS_2$. An orange ellipsoidal crystal with approximate dimensions $0.260 \times 0.165 \times 0.143\ mm^3$ was placed and optically centered on the Bruker SMART CCD system at $-80°C$. The initial unit cell was indexed using a least-squares analysis of a random set of reflections collected from three series of 0.3° wide ω scans (25 frames/series) that were well distributed in reciprocal space. Data frames were collected [Mo$K\alpha$] with 0.3° wide ω scans, 15 s/frame, 606 frames per series, 6 complete series, and an additional 60 frames of the first series for decay purposes, a crystal to detector distance of 3.95 cm, providing a complete sphere of data to $2\theta_{max} = 65.0°$. A total of 8966 reflections were collected and corrected for Lorentz and polarization effects and absorption using Blessing's method as incorporated into the program SADABS with 829 unique [R(int) = 0.0333].

System symmetry and systematic absences were consistent with the noncentrosymmetric orthorhombic space group $Pna2_1$ (No. 33) and the centrosymmetric space group *Pnma* (No. 62). Intensity statistics clearly favored the centric space group. The structure was determined by direct methods with the successful location of nearly all atoms using the program XS (21). The structure was refined with XL (22). The occupancies of the mixed Ba/Sr site were constrained to sum to one, modeling with EADP and EXYZ, but were freely refined as isotropic ions. Convergence resulted in the populations 95% Ba and 5% Sr. Subsequently, the occupancies were fixed at 93% Ba and 7% Sr, based on the analytical data, which resulted in no appreciable change in R factors. In the final cycles of refinement, all atoms were refined anisotropically. The final structure was refined to convergence [$\Delta/\sigma \leq 0.001$] with $R(F) = 1.75\%$, $wR(F^2) = 3.58\%$, and GOF = 1.053 for all 829 unique reflections [$R(F) = 1.55\%$, $wR(F^2) = 3.63\%$ for those 759 data with $F_0 > 4\sigma(F_0)$]. A final difference-Fourier map contained a few peaks, $|\Delta\rho| \leq 1.45\ eÅ^{-3}$, which, upon various refinement attempts, proved to be spurious indicating that the structure is both correct and complete.

Magnetic susceptibilities were measured as a function of temperature and applied magnetic field using a Quantum Design (MPMS) superconducting quantum interference device (SQUID) magnetometer. Samples were weighed, loaded into gelatin capsules (1 cm long, radius = 0.25 cm), and inserted into the magnetometer. The samples were cooled from room temperature to 5 K and a 100-Oe field was applied. The change in magnetization (M) with temperature is measured as the sample is warmed. This process is referred to as zero field cooled (ZFC). Subsequently, the magnetization of samples was recorded as the samples were cooled back to 5 K in the presence of the 100-Oe field (FC-cooling) and as the samples were warmed back to room temperature (FC-warming).

Energy dispersive X-ray spectroscopic analysis (EDX) and wavelength dispersive spectroscopic analysis (WDS) were performed on a JEOL JXA-8900 microprobe analyzer. $BaMnS_2$ and $SrVO_3$ were used as standards for the WDS experiments.

RESULTS

$BaMnS_2$ and $Ba_{0.93}Sr_{0.07}MnS_2$ were prepared by heating stoichiometric amounts of binaries and elements with intermediate regrindings. Several compositions within the $Ba_{1-x}Sr_xMnS_2$ solid solution were attempted, but only 7% Sr substitution could be achieved. At higher substitution levels, biphasic mixtures of $Ba_{0.93}Sr_{0.07}MnS_2$, SrS and MnS were obtained. In addition, a mixture of composition "$SrMnS_2$" was fired at ~2500°C in an argon plasma (dc arc melting), however, XRD analysis of the final product showed only SrS and MnS.

EDX analysis on the $Ba_{1-x}Sr_xMnS_2$ compounds ($x \leq 0.1$) confirmed that Sr had been incorporated into the structure. WDS analysis was performed on single crystals of the $Ba_{0.93}Sr_{0.07}MnS_2$ end member (i.e., maximum Sr substitution) obtained from a synthesis composition containing 10% Sr. The analysis indicated that the limiting composition was $Ba_{0.93}Sr_{0.07}MnS_2$, which was confirmed by single-crystal X-ray diffraction. The results of the crystallographic and WDS compositional analyses are given in Table 1 and are in excellent agreement.

Rietveld analysis of the XRD data for $BaMnS_2$ and $Ba_{0.93}Sr_{0.07}MnS_2$ yielded crystallographic parameters in good agreement with the single-crystal studies of Schmitz and Bronger (16, 17) and our single-crystal studies described herein. The data from the different studies are summarized

TABLE 1
Analytical Data for $Ba_{0.93}Sr_{0.07}MnS_2$

	WDS	Single crystal[a]
Ba	0.93 ± 0.01	0.95
Sr	0.076 ± 0.002	0.05
Mn	1.0 ± 0.01	1
S	2.0 ± 0.01	2

[a] Occupancies based on free refinement of the single crystal XRD data. The occupancies were fixed at the WDS values in the final cycles of refinement of the single crystal structure.

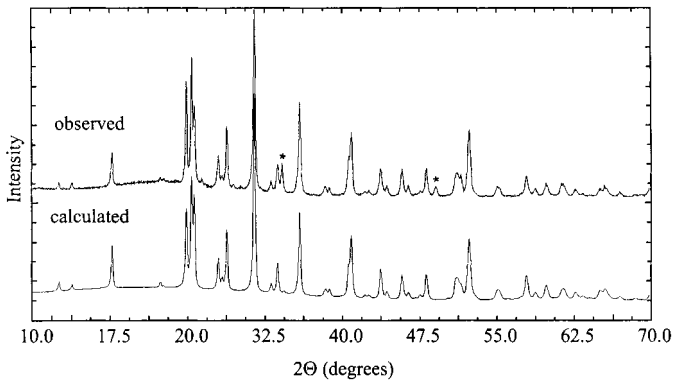

FIG. 1. Observed and calculated (Rietveld analysis) XRD patterns for $Ba_{0.93}Sr_{0.07}MnS_2$. The MnS impurity is indicated with asterisks.

in Table 2. In both compounds, there is a small amount of an MnS impurity phase (~5%). The calculated and observed XRD pattern for $Ba_{0.93}Sr_{0.07}MnS_2$ is shown in Fig. 1 as an example. MnS has been shown to be an antiferromagnet with $T_N = 152$ K (23) and does not complicate the analysis of the magnetic data.

$Ba_{0.93}Sr_{0.07}MnS_2$ and $BaMnS_2$ are isomorphic with *Pnma* crystal symmetry and virtually identical cell parameters (see Table 2). A listing of fractional coordinates and a summary of the crystallographic data for $Ba_{0.93}Sr_{0.07}MnS_2$ are given in Tables 3 and 4, respectively. An ORTEP drawing of the structure is shown in Fig. 2a. A listing of bond distances and angles for $Ba_{0.93}Sr_{0.07}MnS_2$ and Schmitz and Bronger's $BaMnS_2$ (17) is given in Table 5 for comparison. A ball-and-stick drawing illustrating the differences between $Ba_{0.93}Sr_{0.07}MnS_2$ and $BaMnS_2$ is given in Fig. 2b.

The $BaMnS_2$ structure type is characterized by a two-dimensional array of corner sharing $MnS_{4/2}$ tetrahedra extending in the *a*–*b* plane with Mn–S distances of 2.41 Å (av) for both compounds. The range of S–Mn–S angles (Table 5) shows that the $MnS_{4/2}$ units are distorted from idealized tetrahedral geometry but are similar to one another. The Ba^{2+} ions in $BaMnS_2$ are in a seven-coordinate capped trigonal prismatic geometry (Ba–S contacts in the range 3.15–3.47 Å, 3.22 Å av) with an additional long Ba–S contact of 3.97 Å (i.e., 7 + 1 coordination). In the $Ba_{0.93}Sr_{0.07}MnS_2$ compound, the Ba^{2+}/Sr^{2+} coordination is notably altered (Fig. 2b). The composite Ba^{2+}/Sr^{2+} site is shifted to one side of the coordination polyhedron which results in little overall change in the average seven (Ba^{2+}/Sr^{2+})–S distances (3.18–3.40 Å, 3.22 Å av). However, the eighth long contact is lengthened to 4.12 Å and can be considered nonbonding.

Magnetic Properties

The susceptibility of $BaMnS_2$ at 100 Oe between 5 and 380 K is shown in Fig. 3. It is essentially temperature independent between 200 and 380 K and decreases slightly with temperature below 220 K. The change in magnetization with field at 5 and 200 K is shown in Fig. 4. Both plots are linear and the slope decreases with decreasing temperature. The linearity and the absence of saturation indicate that the compound is weakly antiferromagnetic at these temperatures. The absence of an apparent transition to the antiferromagnetic state in the plot of susceptibility vs temperature suggests that the Neel temperature is higher than 380 K. However, higher temperature susceptibility studies are

TABLE 2
Unit Cell Dimensions of Orthorhombic (*Pnma*) $BaMnS_2$ and $Ba_{0.93}Sr_{0.07}MnS_2$

	$BaMnS_2$[a]	$BaMnS_2$[b]	$Ba_{0.93}Sr_{0.07}MnS_2$[b]	$Ba_{0.93}Sr_{0.07}MnS_2$[c]
a (Å)	7.00(0)	7.109(2)	7.119(2)	7.109(2)
b (Å)	4.14(4)	4.124(1)	4.121(1)	4.1069(13)
c (Å)	14.00	13.991(3)	13.960(3)	13.938(4)
V (Å^3)	405.7	410.2(2)	409.5(2)	407.0(2)
d (g/cm^3)	4.19	4.15	4.10	4.13

[a] Room temperature single crystal data from Ref (17).
[b] Room temperature data from Rietveld analysis of powder XRD data (this work).
[c] Single crystal data recorded at 193 K (this work).

TABLE 3
Atomic Coordinates ($\times 10^4$) and Equivalent Isotropic Displacement Parameters (Å$^2 \times 10^3$) for $Ba_{0.93}Sr_{0.07}MnS_2$[a]

	x	*y*	*z*	*U*(eq)[b]
Ba	2027(1)	2500	6299(1)	9(1)
Sr	2027(1)	2500	6299(1)	9(1)
Mn	2791(1)	2500	3662(1)	8(1)
S(1)	− 385(1)	− 2500	7570(1)	9(1)
S(2)	− 2435(1)	2500	5429(1)	12(1)

[a] All atoms reside on Wyckoff 4c sites ($x, \frac{1}{4}, z$).
[b] *U*(eq) is defined as one-third of the trace of the orthogonalized U^{ij} tensor.

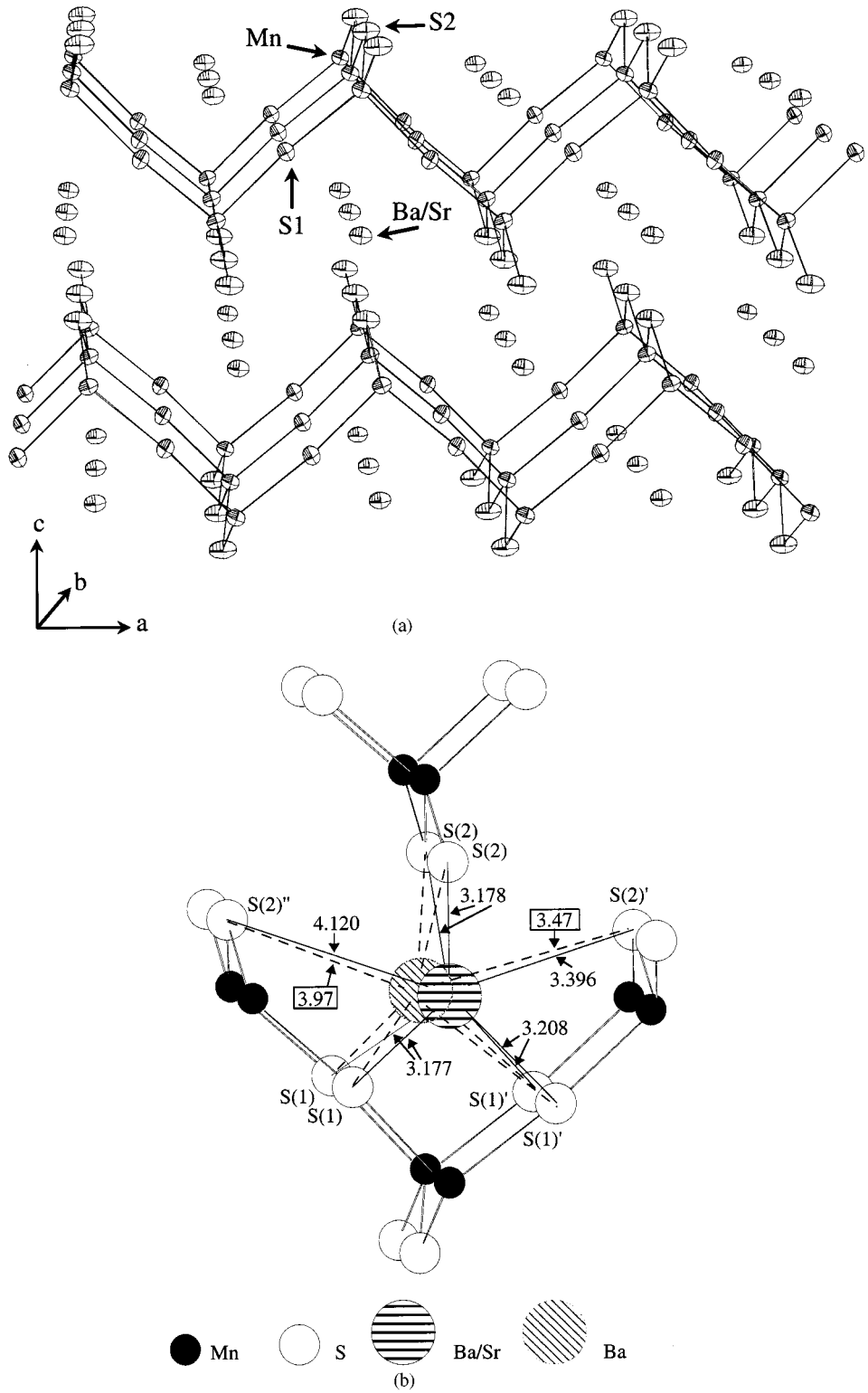

FIG. 2. (a) ORTEP drawing of the $Ba_{0.93}Sr_{0.07}MnS_2$ structure. (b) Superposition of the $Ba_{0.93}Sr_{0.07}MnS_2$ and $BaMnS_2$ structures illustrating the differences in Ba and Ba/Sr coordination in the two phases. The dotted lines and the distances in the boxes correspond to $BaMnS_2$.

TABLE 4
Crystal Data and Structure Refinement for $Ba_{0.93}Sr_{0.07}MnS_2$

Empirical formula	$Ba_{0.93}MnS_2Sr_{0.07}$
Formula weight	252.92
Temperature	193(2) K
Wavelength	0.71073 Å
Crystal system	Orthorhombic
Space group	*Pnma*
Unit cell dimensions	$a = 7.109(2)$ Å
	$b = 4.1069(13)$ Å
	$c = 13.938(4)$ Å
Volume	407.0(2) Å^3
Z	4
Density (calculated)	4.128 g/cm^3
Absorption coefficient	13.743 mm^{-1}
Data/restraints/parameters	829/0/26 [R(int) = 0.0333]
Goodness-of-fit on F^2	1.072
Final R indices [$I > 2\sigma(I)$]	$R1 = 0.0155$, w$R2 = 0.0358$
R indices (all data)	$R1 = 0.0175$, w$R2 = 0.0363$
Extinction coefficient	0.0028(3)
Largest diff. peak and hole	1.451 and -0.720 e Å^{-3}

Note. $R(F) = \sum\| F_o| - |F_c\|/\sum|F_o|$ and $wR(F^2) = [\sum[w(F_o^2 - F_c^2)^2]/\sum[w(F_o^2)^2]]^{1/2}$. The parameter $w = 1/[\sigma^2(F_o^2) + (0.0326 * P)^2 + 8.5143 * P]$, with $P = (F_o^2 + 2F_c^2)/3$.

necessary to confirm this proposal. The magnitude of the molar susceptibility at all temperatures is less than that expected from a high spin Mn^{2+} system ($\sim 5.9\ \mu_B$ per Mn^{2+}). The supressed susceptibility is most likely due to the weak antiferromagnetic interactions in the compound.

For $Ba_{0.93}Sr_{0.07}MnS_2$, the susceptibility at 100 Oe in the temperature range 5 to 380 K is dependent on the experimental conditions (Fig. 5). In all cases, the data show the

TABLE 5
Comparison of the Selected Bond Angles and Bond Distances for $Ba_{0.93}Sr_{0.07}MnS_2$ and $BaMnS_2$[a]

	$Ba_{0.93}Sr_{0.07}MnS_2$	$BaMnS_2^a$
S(1)′–Mn–S(2)	107.24(2) (2×)	109.29 (2×)
S(1)–Mn–S(2)	114.39(2) (2×)	114.023 (2×)
S(2)–Mn–S(2)	115.64(4)	113.669
S(1)–Mn–S(1)′	95.34(3)	94.766
Mn–S(1)–Mn	174.45(3)	177.865
Mn–S(2)–Mn	115.64(4)	113.669
	(Ba/Sr)–S	Ba–S
Ba–S(1)	3.1768(8) (2×)	3.18 (2×)
Ba – S(2)	3.1777(9) (2×)	3.15 (2×)
Ba–S(1)′	3.2082(8) (2×)	3.22 (2×)
Ba–S(2)′	3.3959(12)	3.47
Ba–S(2)″	4.120(1)	3.97
	Mn–S	Mn–S
Mn–S(1)′	2.3918(9)	2.38
Mn–S(1)	2.4238(9)	2.39
Mn–S(2)	2.4261(7) (2×)	2.47 (2×)

[a] Data from Ref. (17).

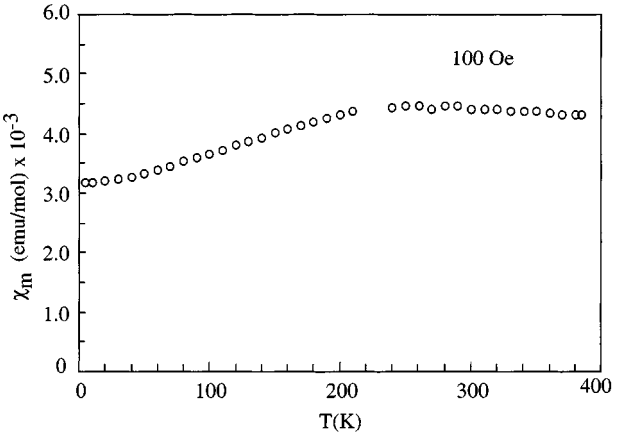

FIG. 3. Molar magnetic susceptibility for $BaMnS_2$ recorded at 100 Oe.

onset of short-range magnetic interactions at 230 K that disappear at 70 K. The susceptibility of the sample as it is warmed is essentially the same whether it is zero field cooled (ZFC) or field cooled (FC). However, the susceptibility is enhanced between 70 and 230 K when measured in the cooling mode (FC—cooling). Above 250 K the magnetization is independent of the experimental conditions. The differences between the FC and ZFC data indicate that the magnetic interactions are not due to long-range ordering. The magnetic anomalies in this region are due to local effects such as local spin canting or uncompensated ferromagnetism. At 70 K the compound undergoes a first-order phase transition back to an antiferromagnetic state and is quite similar to $BaMnS_2$ below this temperature. The room temperature susceptibility for this compound is very close to that of $BaMnS_2$.

Magnetization versus field experiments were conducted for $Ba_{0.93}Sr_{0.07}MnS_2$ at three different temperatures: 5, 100, and 220 K (Fig. 6a). The plots are all linear and do not

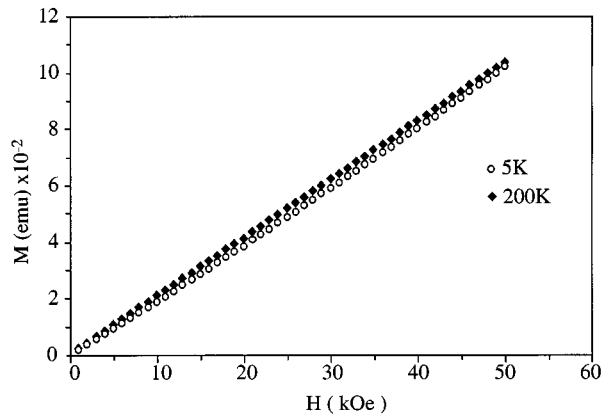

FIG. 4. Magnetization versus field plots for $BaMnS_2$ recorded at 5 and 200 K.

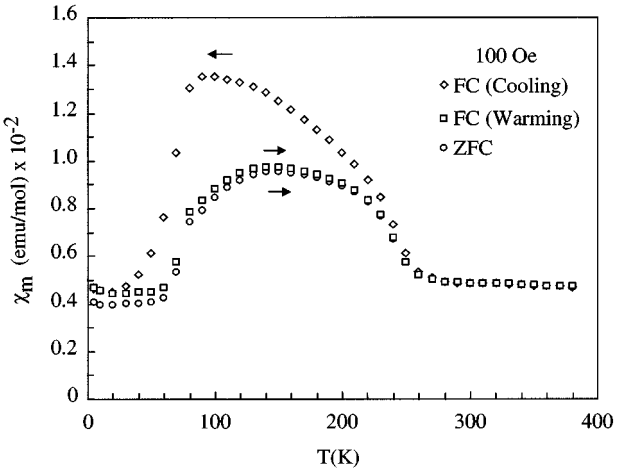

FIG. 5. Molar magnetic susceptibility (zero field cooled, field cooled—cooling, and field cooled—warming) for $Ba_{0.93}Sr_{0.07}MnS_2$ at 100 Oe.

saturate at high fields, suggesting the presence of an antiferromagnetic ordering at these temperatures. The $M(H)$ plot at 100 K appears to be linear even at negative fields (Fig. 6b). On the other hand, the local ordering gives rise to a small hysteresis that is seen at low fields (Fig. 6c).

DISCUSSION

It is interesting to note that, although there are several Ba–M–S compounds of the 3d metals (M = 3d transition metal), a search of the Gemelin database shows that very few ternary Ca–M–S or Sr–M–S phases exist. This phenomenon contrasts the solid state chemistry of the oxides and is surprising in view of the relatively large number of rare earth R–M–S sulfides (24). The present study showed that incorporation of Sr into the $BaMnS_2$ structure could only be accomplished to a minimal extent ($\sim 7\%$) even under the forcing conditions of dc arc melting. However, this small isovalent substitution has a significant effect on the magnetic properties of the material.

The short-range magnetic ordering observed for $Ba_{0.93}Sr_{0.07}MnS_2$ is most likely due to subtle changes in structure resulting from the Sr^{2+}-for-Ba^{2+} substitution in the antiferromagnetic $BaMnS_2$ compound. Although the crystal structure and symmetry for $Ba_{0.93}Sr_{0.07}MnS_2$ at 298

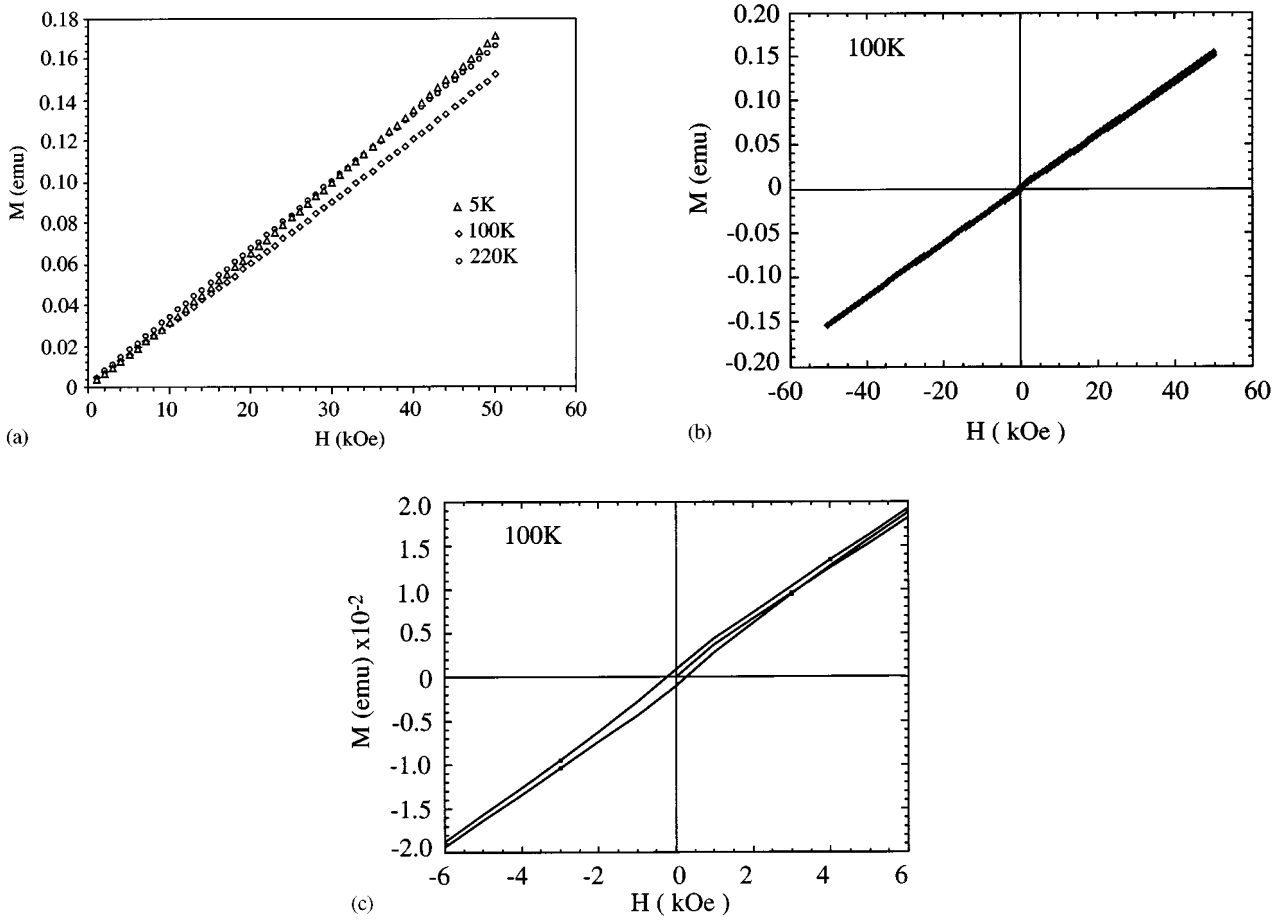

FIG. 6. Magnetization versus field plots of $Ba_{0.93}Sr_{0.07}MnS_2$ (a) at 5, 100, and 220 K, (b) at 100 K in the field range -50 to 50 kOe, and (c) at 100 K in the field range -6 to 6 kOe.

and 193 K are the same as those for $BaMnS_2$, the Sr^{2+} ion resides in a position slightly off center from that of the Ba^{2+} ion in $BaMnS_2$. This shift in position is due to the poor fit of Sr^{2+} in the Ba^{2+} coordination sphere, as was seen in the $Ba_{1-x}Sr_xZrSe_3$ phases (25), and may be responsible for the short-range magnetic correlations in the title compound.

ACKNOWLEDGMENTS

We thank Professor J. Gopalakrishnan and Dr. Vera Smolyaninova for helpful discussions and Mr. Scott Sircho for the WDS analysis. We also thank a reviewer for pointing out the possibility of ferrimagnetic interactions.

REFERENCES

1. B. Raveau, A. Maignan, C. Martin, and M. Hervieu, *Chem. Mater*. **10,** 2641 (1998).
2. T. O. Ozawa, S. L. Brock, S. M. Kauzlarich, and D. M. Young, *Chem. Mater*. **10,** 392 (1998).
3. J. Y. Chan, M. E. Wang, A. Rehr, S. M. Kauzlarich, and D. J. Webb, *Chem. Mater*. **9,** 2131 (1997).
4. J. Y. Chan, S. M. Kauzlarich, P. Klavins, R. N. Shelton, and D. J. Webb, *Chem. Mater*. **9,** 3132 (1997).
5. J. Y. Chan, S. M. Kauzlarich, P. Klavins, R. N. Shelton, and D. J. Webb, *Phys. Rev. B* **57,** R8103 (1998).
6. Y. Shimakawa, Y. Kubo, and T. Manako, *Nature* **379,** 53 (1996).
7. M. A. Subramanian, B. H. Toby, A. P. Ramirez, W. J. Marshall, A. W. Sleight, and G. H. Kwei, *Science* **273,** 81 (1996).
8. J. Kim and T. Hughbanks, *J. Solid State Chem.* **146,** 217 (1999).
9. J. Y. Kim, C. C. Wang, and T. Hughbanks, *Inorg. Chem.* **38,** 235 (1999).
10. A. P. Ramirez, R. J. Cava, and J. Krajewski, *Nature* **386,** 156 (1997).
11. C. F. van Bruggen, M. B. Vellinga, and C. Haas, *J. Solid State Chem.* **2,** 303 (1970).
12. S. Gonen, P. Fournier, V. Smolyaninova, R. L. Greene, F. M. Araujo-Moreira, and B. Eichhorn, *Chem. Mater*., in press, 2000.
13. W. Bronger, *Angew. Chem. Int. Ed. Engl.* **20,** 52 (1981).
14. W. Bronger, U. Hendriks, and P. Müller, *Z. Anorg. Allg. Chem.* **559,** 95 (1988).
15. W. Bronger, H. Balk-Hardtdegen, and D. Schmitz, *Z. Anorg. Allg. Chem.* **574,** 99 (1989).
16. D. Schmitz and W. Bronger, *Naturwissenschaften* **58,** 332 (1971).
17. D. Schmitz and W. Bronger, *Z. Anorg. Allg. Chem.* **402,** 225 (1973).
18. M. A. Greaney, K. V. Ramanujachary, Z. Teweldemedhin, and M. Greenblatt, *J. Solid State Chem.* **107,** 554 (1993).
19. I. E. Grey and H. Steinfink, *Inorg. Chem.* **10,** 691 (1971).
20. L. J. Tranchitella, J. C. Fettinger, and B. W. Eichhorn, *Chem. Mater*. **8,** 2265 (1996).
21. G. M. Sheldrick, SHELXTL, Siemens Analytical X-Ray Instruments, Inc., Madison, WI, 1994.
22. G. M. Sheldrick, *Acta Crystallogr. A* **46,** 467 (1990).
23. C. N. R. Rao and K. P. R. Pisharody, *Prog. Solid State Chem.* **10,** 207 (1976).
24. B. W. Eichhorn, *in* "Progress in Inorganic Chemistry" (K. D. Karlin, Ed.), Wiley & Sons, New York, 1994.
25. L. Tranchitella, B. H. Chen, J. C. Fettinger, and B. W. Eichhorn, *J. Solid State Chem.* **130,** 20 (1997).